Remote Sensing of Environment 210 (2018) 1–11

Contents lists available at ScienceDirect

Remote Sensing of Environment

journal homepage: www.elsevier.com/locate/rse

Remote sensing of surface [nitrite + nitrate] in river-influenced shelf-seas: The northern South China Sea Shelf-sea

Xiaoju Pan[a,*], George T.F. Wong[b,c], Tung-Yuan Ho[b], Jen-Hua Tai[b], Hongbin Liu[d], Juanjuan Liu[a], Fuh-Kuo Shiah[b]

[a] Key Laboratory of Marine Chemistry Theory and Technology, Ocean University of China, Ministry of Education, Qingdao, Shandong, China
[b] Research Center for Environmental Changes, Academia Sinica, Taipei, Taiwan
[c] Department of Ocean, Earth and Atmospheric Sciences, Old Dominion University, Norfolk, VA, USA
[d] Division of Life Science, Hong Kong University of Science and Technology, Hong Kong

ARTICLE INFO

Keywords:
Remote sensing
Nitrite
Nitrate
Color dissolved organic matter
Sea surface temperature
River-influenced shelf-sea
Northern South China Sea

ABSTRACT

Sea surface concentrations of [nitrite + nitrate], [N + N], have been assessed successfully by remote sensing in the open oceans by utilizing its relationship to sea surface temperature (SST). A similar approach was not met with similar success in the river-influenced shelf waters in the northern South China Sea Shelf-sea (NoSoCS) where riverine inputs, in which the relationship between the concentration of [N + N] and SST was not straight forward, are significant. By considering river-influenced shelf waters as a mixture of open ocean water and riverine inputs and then combining SST with the absorption coefficient of colored dissolved organic matter (CDOM) at 412 nm, $a_g(412)$, which serves as an indicator of the riverine influence, an algorithm has been developed for remotely sensing the surface concentration of [N + N] in the NoSoCS. This satellite-derived concentration of [N + N] was validated by direct observations. In 16 match-up comparisons within a time window of ± 24 h and concentrations of [N + N] ranging between 0.2 and 74 μM, the uncertainty was ± 40%. The climatological distributions of the derived concentration of [N + N] in the NoSoCS and surrounding waters between 2002 and 2014 are consistent with the reported distributions based on ship-board observations. Thus, as a result of riverine inputs, the concentration of [N + N] generally increases towards the coasts, varying by more than two orders of magnitude from about 0.5 μM and near zero in the open northern South China Sea (NSCS) in January and July respectively to about 50 and 100 μM at the mouth of the Pearl River. In the open NSCS where nutrient availability is controlled primarily by the enhanced winter convective overturn, the intra-annual variations in the concentration of [N + N] follow a distinct seasonal cycle, reaching a minimum close to zero in the summer and a maximum, 0.7 μM, in the winter. In the NoSoCS, as a result of the high riverine input of nutrients in the summer, in addition to the maximum in the winter, there is a secondary summer maximum, which becomes increasingly prominent towards the coast. This work represents a first attempt to characterize the distributions of the surface concentration of [N + N] in river-influenced shelf-seas from space. With appropriate regional tuning, a similar approach may be applicable to other river-influenced shelf-seas such as the Texas-Louisiana Shelf.

1. Introduction

The shelf-seas contribute disproportionately to marine primary production which plays an important role in global marine carbon cycle. They account for about 22% of the global marine production although they cover only 7% of the area of the global oceans (Cai, 2011; Chen, 2003; Pauly and Christensen, 1995). Among the shelf-seas, those that receive significant riverine inputs, designated as the river-influenced shelf-seas here, such as the East China Sea, the northern South China Sea Shelf-sea and the Texas-Louisiana Shelf, are in turn an important subset (Cai, 2011; Cai and Dai, 2004; Cai et al., 2014; Lohrenz et al., 2014; Thomas et al., 2004). These shelf-seas receive the outflows of some of the world's major rivers, the Changjiang River, the Pearl River and the Mississippi River respectively in these three cases, and the riverine inputs can lead to especially elevated biological production and they have frequently been referred to as river-dominated systems (Chou et al., 2017; Huang et al., 2015; Liu et al., 2012; Rabouille et al., 2008).

Since the availability of combined nitrogen, mainly nitrite and

* Corresponding author.
E-mail address: xpan@ouc.edu.cn (X. Pan).

https://doi.org/10.1016/j.rse.2018.03.012
Received 2 October 2016; Received in revised form 4 January 2018; Accepted 7 March 2018

nitrate, is an important control of biological production in the marine environment (Hecky and Kilham, 1988; Yin et al., 2014), the surface distribution of the concentration of [nitrite + nitrate], [N + N], can provide important clues on the spatial variability in biological production in the oceans. Thus, the surface concentrations of [N + N] are generally low in the less productive ocean interior, and higher in the more productive land margin (Levitus et al., 2014; Moore et al., 2013; Rousseaux and Gregg, 2015). In recent years, the riverine input of nutrients has increased noticeably as anthropogenic activities in the river basins increase (Bonsdorff et al., 1997; Levitus et al., 2014; Strokal et al., 2014; Wakelin et al., 2015). In some river-influenced shelf-seas, these increasing riverine inputs of nutrients have led to deleterious ecological consequences, such as eutrophication, harmful algal bloom and hypoxia, in the coastal zones (Gilbert et al., 2014; Li et al., 2015; Strokal et al., 2014; Wakelin et al., 2015).

Traditionally, the surface distribution of the concentration of [N + N] is constructed from the concentrations obtained in discrete water samples collected during individual cruises (Cai et al., 2004; Hong et al., 2011; Levitus et al., 2014; Wong et al., 2015a). However, such data bases are usually limited in their spatial and/or temporal coverage. Satellite remote sensing has been used for some years to augment the direct field observations as it can provide a synoptic view of large regions of the oceans continuously over years to decades. The algorithm for estimating the concentration of [N + N] by remote sensing is based on the well-established negative correlation between the concentration of [N + N] and temperature when [N + N] in the surface waters originates predominantly from the cold and [N + N]-replete subsurface water as a result of vertical mixing (Goes et al., 2000; Kamykowski et al., 2002; Switzer et al., 2003). With regional tuning, this algorithm has been applied successfully to the major ocean basins and to upwelling zones. The uncertainty in the satellite-derived concentration of [N + N] is about ± 33% (Switzer et al., 2003). Further refinements, by incorporating additional hydrographic parameters, such as chlorophyll *a* concentration and mixed layer depth, into the algorithm, have been proposed (Arteaga et al., 2015; Goes et al., 2000). While most of the previous studies focused primarily on remotely sensing the distribution of surface [N + N] in the major ocean basins, Hutahaean et al. (2010) and Silió-Calzada et al. (2008) reported the use of the combination of SST and chlorophyll *a* for assessing the distribution of surface [N + N] in a coastal marine bay and in an upwelling zone respectively.

Despite of their successes, these algorithms have not been applied extensively to, and may not be appropriate for, the river-influenced shelf-seas where riverine inputs of [N + N] may be significant and sub-regionally variable and the relationship between the concentration of [N + N] and temperature may not be straight forward (Cai et al., 2004; Levitus et al., 2014; Switzer et al., 2003; Wong et al., 2015a). If, as a first approximation, the [N + N] in the river-influenced shelf-seas can be regarded to be originated predominantly from vertical mixing and riverine inputs only, a possible avenue for accommodating the influence of the latter is to incorporate an additional remotely sensed proxy for it into the algorithm and a good candidate for this purpose is colored dissolved organic matter (CDOM). The concentration of CDOM is known to be higher in river water than in seawater and its absorption can be remotely sensed (Bai et al., 2013; Callahan et al., 2004; Dong et al., 2013; Mannino et al., 2008, 2014; Pan et al., 2008). The remotely sensed CDOM absorption has been successfully used for estimating salinity and dissolved organic carbon (DOC), which are good indicators of riverine influence, in the shelf-seas (Bai et al., 2013; Mannino et al., 2008; Pan and Wong, 2015). Pan and Wong (2015) reported that the seasonal tuning required in the estimation of DOC from CDOM absorption alone can be circumvented by incorporating SST into the algorithms.

In this study, we report a first attempt to develop an algorithm for the estimation of the surface concentration of [N + N] in the river-influenced shelf-seas by using remotely sensed sea surface temperature (SST) and CDOM absorption. The algorithm has been applied to the northern South China Sea Shelf-sea (NoSoCS) and adjacent waters in order to assess the climatology in the distributional pattern and the intra-annual variations in the surface concentration of [N + N] in the region.

2. Data and methods

2.1. Study area

The NoSoCS is a broad and extensive river-influenced shelf system in the northern South China Sea (NSCS) (Liu et al., 2012; Rabouille et al., 2008), covering an area of ~1.6×10^5 km^2 between the southern coast of China and the 120-m isobaths offshore and between the southern end of the Taiwan Strait and the coasts of the northeastern Leizhou Peninsula and the Hainan Island (Fig. 1). It may be subdivided into three hydrographic regimes: the inner, middle and outer shelf at water depths of < 40 m, 40–90 m and 90–120 m, respectively (Wong et al., 2015a, 2015b). The biogeochemical characteristics of the inner shelf are heavily influenced by riverine inputs while those in the outer shelf are mainly determined by its interactions with the upper water in the adjoining open NSCS further offshore (Callahan et al., 2004; Guo et al., 2008; Ho et al., 2015; Liu et al., 2002, 2013; Pan et al., 2015; Tseng et al., 2005; Wong et al., 2015a, 2015b; Yin, 2002). Intra-annual variations in the NoSoCS are driven to a large extent by the monsoons as the strong northeast monsoonal wind is found between November and April and the weaker southwest monsoonal wind is found between June and August (Liu et al., 2002; Pan et al., 2015; Tseng et al., 2005). These two monsoonal seasons are separated by short inter-monsoonal periods in May and September–October.

In the upper waters in the open NSCS, below about 23 °C, the concentration of [N + N] is negatively correlated to water temperature and the relationship is controlled by vertical mixing (Wong et al., 2007, 2015a) as found in the open oceans. The intra-annual variations in the intensity of the vertical mixing in the NCSC is primarily controlled by the combined effect of monsoonal wind forcing and surface cooling/heating (Liu et al., 2002, 2013; Pan et al., 2015; Tseng et al., 2005). Since the stronger wind is found during the northeast monsoonal season when surface cooling also reaches its peak (Pan et al., 2015), deeper mixed layer depths and higher surface concentrations of [N + N] are found during the winter months (Wong et al., 2007, 2015a).

The dominant source of riverine input to the NoSoCS is the outflow from the Pearl River and it plays a major role in shaping the biogeochemical and physical characteristics in the NoSoCS, and especially in its inner shelf (Gan et al., 2009, 2010; Guo et al., 2008; Pan et al., 2015). The negative correlations observed between both CDOM and the concentration of [N + N] and salinity in the inner and middle shelf of the NoSoCS have been attributed to the mixing between the Pearl River water, which is enriched in both, with the water from the outer shelf and the open NSCS (Callahan et al., 2004; Chen et al., 2004a; Pan and Wong, 2015; Pan et al., 2015; Wong et al., 2015a; Yin, 2002). Since the discharge from the Pearl River reaches its maximum during the summer months when the temperature in the NoSoCS is generally higher during the year (Guo et al., 2008; Pan et al., 2015), the concentration of river-derived [N + N] will be positively correlated rather than negatively correlated with temperature as in the open NSCS. Furthermore, to a certain degree, the river-derived [N + N] will also be temporally segregated from the [N + N] supplied by vertical mixing, which reaches a maximum in the winter. Pan et al. (2015) reported that, in response to the availability of these two sources of nutrients, a maximum in the concentration of chlorophyll *a* can be found both in the winter and in the summer in the NoSoCS, and the summer maximum is increasingly more prominent towards the coast as riverine influence increases. Coastal upwelling is another source of [N + N] to some sub-regions in the NoSoCS. Upwelling has been reported to occur year round around the Taiwan Bank (Hu et al., 2010; Pan et al., 2015). However, the

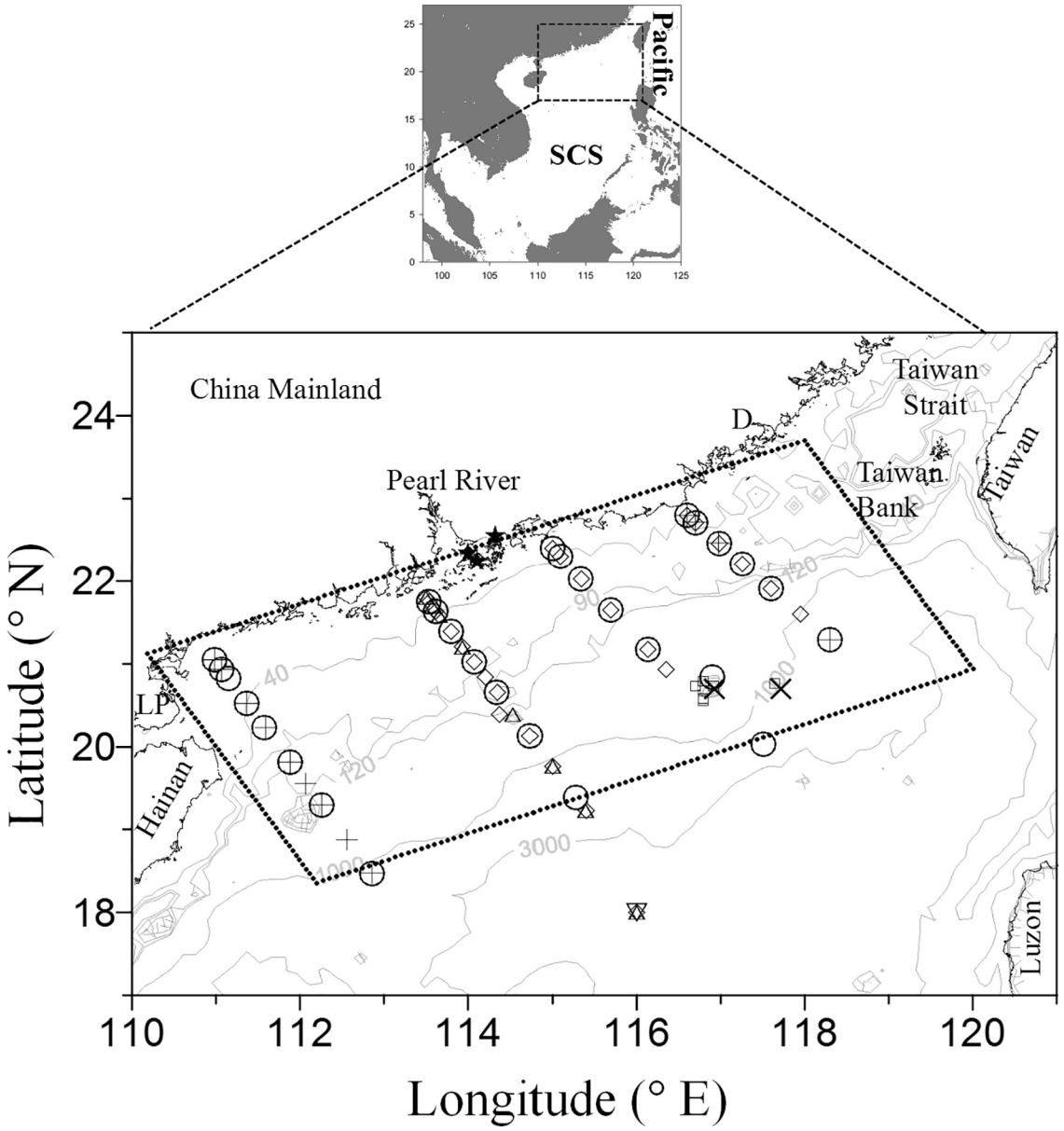

Fig. 1. The study area within the South China Sea (SCS) and the station locations in the Northern South China Sea Shelf-sea (NoSoCS) and adjacent waters during cruises OR1-0929 (○), OR1-0944 (▽), OR1-0953 (+), OR1-1053 (△), OR3-1770 (x), OR1-1084 (◊) and OR1-1095 (□). ★ – the three stations off Hong Kong; LP – Leizhou Peninsula; D – Dongshan. The monthly average concentration of [N + N] and SST in the different hydrographic sub-divisions shown in Fig. 8 were estimated in the area enclosed by the dotted lines.

elevated concentration of [N + N] in the upwelling waters has been found to be negatively correlated with temperature (Wang et al., 2013; Wong et al., 2015a) as in the open oceans.

2.2. Field in situ observations for the development of an algorithm for [N + N]

Stations were occupied in the NoSoCS and adjacent waters during seven cruises between 2010 and 2014: OR1-0929 (3 to 12 June 2010), OR1-0944 (13 to 15 October 2010), OR1-0953 (30 December 2010 to 7 January 2011), OR1-1053 (16 to 19 October 2013), OR3-1770 (4 to 7 June 2014), OR1-1084 (5 to 11 August 2014) and OR1-1095 (19 to 22 November 2014) (Fig. 1). At each station, the vertical distributions of water temperature and salinity were recorded with a conductivity-temperature-depth (CTD) recorder (SeaBird SBE9/11). Discrete water samples were collected with depth by using 20-L Go-Flo bottles mounted onto a Rosette sampling assembly (General Oceanic). Subsamples for the determination of CDOM were filtered through 0.2 μm Whatman Nuclepore® filters onboard ship and stored at 4 °C. Following the sample collection protocol of the Joint Global Ocean Flux Study (JGOFS, 1994), water samples for the determination of [N + N], unfiltered for the open ocean waters but filtered with GF/F filters for the coastal waters, were collected in 100-mL bottles, quick frozen in liquid nitrogen and stored frozen at −20 °C. All these samples were returned to a shore-based laboratory at Academia Sinica for further analyses.

In the laboratory, the absorption of CDOM was measured by following the method of Mitchell et al. (2002). The absorbance of each sample in a 10-cm quartz cell relative to Milli-Q water was recorded between 280 and 800 nm in 1-nm intervals by using a Perkin Elmer Model Lambda 850 UV/Vis spectrophotometer. The spectral absorption coefficient of CDOM, $a_g(\lambda)$, is calculated as:

$$a_g(\lambda) = 2.303[A(\lambda)]/L \quad (1)$$

where $A(\lambda)$ is the absorbance at a wavelength λ after correcting for the null value, which is the mean absorbance between 675 and 685 nm, and L is the cell path-length, or 0.1 m. The precision in the determination of

$a_g(\lambda)$ was about ± 0.01 m^{-1}. CDOM is expressed as $a_g(412)$ (Mannino et al., 2008, 2014; Pan and Wong, 2015). The concentration of [N + N] was determined by the standard pink azo dye method which has been adapted for use with a flow injection analyzer (Pai et al., 1990; Strickland and Parsons, 1972). The precision was about ± 0.1 μM and thus the concentrations of [N + N] below 0.1 μM were practically undetectable.

Additional concentrations of [N + N] and the corresponding $a_g(412)$ in the Pearl River estuary in July 1999 (Cruise PRE-1999) were extracted from the published literature. The concentrations of [N + N] and the corresponding salinity, water temperature and $a_g(355)$ were taken from Chen et al. (2004a, 2004b). Then, $a_g(355)$ was converted to $a_g(412)$ following the method of Pan and Wong (2015).

Only 142 out of 144 data points, where both [N + N] and $a_g(412)$ were measured, were used in the development of the algorithm. The remaining 2 data points, which matched with the satellite observations, were used only for the validation of the algorithm.

2.3. Field in situ observations for the validation of the algorithm

The concentrations of [N + N] in the surface waters at different locations in the study area within a time window of ± 24 h from an overpass of the MODerate resolution Imaging Spectroradiometer on Aqua (MODIS-Aqua) were drawn from four different sources: (1) from the field observational program of this study in the NoSoCS as described in Section 2.2; (2) from the SouthEast Asian Time-series Study (SEATS) data bank at the Research Center for Environmental Changes, Academia Sinica at the SEATS station (~116° E, 18° N) (Wong et al., 2007); (3) from the data bank of the Division of Life Science of the Hong Kong University of Science and Technology at three stations off Hong Kong: the East Lamma Channel Station (114.11° E, 22.24° N), the West Lamma Channel Station (114.00° E, 22.34° N) and the Round Island Station (114.33° E, 22.55° N) (Fig. 1); and (4) from published literatures (Chen et al., 2013; Huang et al., 2011) where results from observations made at the NoSoCS were reported. All stations in these four sources were at least 10 km away from the coast so that the satellite-derived remote sensing reflectance (R_{rs}) spectra might be sufficiently free from the interference of land and might be used reliably for the derivation of the absorption coefficient of CDOM. In fact, even at the three stations off Hong Kong, which were nearest to the coast (Fig. 1), the R_{rs} found agreed reasonably well with those observed *in situ* in coastal waters of a similar optical type as defined by Wei et al. (2016) (unpublished data). The data in these four sources were collected between 2002 and 2014, and only the data points whose field observed concentrations of [N + N] were > 0.1 μM were used. By pooling the data from these four sources, a total of 16 match-up comparisons between observed and remotely sensed concentrations of [N + N] could be made. They covered both monsoonal seasons and a concentration range of 0.2 to 74 μM.

2.4. Satellite imagery

Daily Level-2 products of remote sensing reflectance at 488 and 555 nm, $R_{rs}(488)$ and $R_{rs}(555)$, and night-time (4 μm) SST obtained by the MODIS-Aqua between 2002 and 2014 covering the area of 17–25° N and 110–121° E, were downloaded from the NASA Ocean Color Web (http://oceancolor.gsfc.nasa.gov/). Pan and Wong (2015) have reported an empirical global relationship, which was constructed from the NOMAD (NASA bio-Optical Marine Algorithm Data) data-base, for estimating $a_g(412)$ from $R_{rs}(488)$ and $R_{rs}(555)$ such that:

$$\log[a_g(412)] = -0.8313 - 1.884X + 0.4732X^2 \quad (2)$$

Here $X = \log[R_{rs}(488)/R_{rs}(555)]$. The root mean square error ($RMSE_{log}$) in the estimated $\log[a_g(412)]$ and the mean absolute percentage difference (MAPD) in the estimated $a_g(412)$ were about ± 0.208 and ± 40%, respectively. Since *in situ* observational data in the NoSoCS are not yet available for constructing a site-specific relationship, $a_g(412)$ was estimated in each pixel by using this global empirical relationship. Satellite images were mapped isotropically to 111 pixels per degree of longitude or latitude, corresponding to an approximate spatial resolution of 1 × 1 km^2 per pixel, by using the SeaWiFS Data Analysis System software (SeaDAS; v6.4). Then, the satellite-derived SST and $a_g(412)$ were used to calculate the concentration of [N + N] in each pixel by following the approach developed in this study. The daily mapped images in the distribution of the concentration of [N + N] were arithmetically binned step-by-step to get the monthly and climatological monthly distributions.

2.5. Statistics

The performance of the algorithm and the validation of the remotely sensed concentrations of [N + N] were evaluated by their root mean square error in log form ($RMSE_{log}$) and their mean absolute percentage difference (MAPD) such that:

$$RMSE_{log} = \sqrt{\sum [\log(D) - \log(F)]^2/n} \quad (3)$$

$$MAPD = \sum \frac{|D - F|}{nD} \times 100\% \quad (4)$$

Here, n, D and F were the number of samples, the derived and the field observed concentrations of [N + N], respectively. Following the common practice in evaluating remotely sensed products covering wide ranges in concentration (O'Reilly et al., 1998), the root mean square error was evaluated by a log-transformation, designated as $RMSE_{log}$, in the concentrations of [N + N] so as to generate a normal distribution in the concentration of [N + N]. Field observed concentrations of [N + N] below 0.1 μM were considered undetectable and these data points were excluded from the statistical treatments.

2.6. [N + N], SST and $a_g(412)$ from the Texas-Louisiana Shelf in the northern Gulf of Mexico

The concentrations of [N + N], SST and salinity at the Texas-Louisiana Shelf in the northern Gulf of Mexico were drawn from the National Oceanographic Data Center (NODC), including those collected in the Gulf of Mexico and East Coast Carbon Cruises during July 2007 (GOMECC-1; ftp://ftp.nodc.noaa.gov/nodc/archive/arc0028/0066603/) and July 2012 (GOMECC-2; ftp://ftp.nodc.noaa.gov/nodc/archive/arc0069/0117971/), and the compiled data for the Environmental Protection Agency (EPA) cruises between 2004 and 2008 (ftp://ftp.nodc.noaa.gov/nodc/archive/arc0034/0073142/). The $a_g(412)$ data during GOMECC-2 were also available from the NODC, while the $a_g(412)$ data during EPA cruises in July–September 2007 were extracted from Tehrani et al. (2013).

3. Results and discussions

3.1. Intra-annual and spatial variations in in situ observations

The data from the eight cruises listed in Section 2.2 were separated into those from the northeast monsoonal season in November through April and those from the rest of the year. The average composition of the waters in the top 20 m of the mixed layer in the different hydrographic sub-divisions in the NoSoCS and the adjacent open NSCS in these two periods of time is shown in Table 1. Salinity and water temperature increased, while $a_g(412)$ and the concentration of [N + N] decreased seaward during both time-periods as found previously (Pan and Wong, 2015; Wong et al., 2015a). Compositional changes were abrupt between the inner and middle shelf and relatively minor from the middle shelf to the open NSCS. In the inner shelf, a higher $a_g(412)$ and a higher concentration of [N + N] were found in May through

Table 1
The average composition (± 1 SD) of the waters in the top 20 m of the mixed layer in the different hydrographic sub-divisions in the NoSoCS and the adjacent open NSCS. The statistical analyses were based on the data used for the algorithm development, as described in Section 2.2.

*Parameters	Inner shelf	Middle shelf	Outer shelf	Open NSCS
November to April – Northeast monsoon				
Stations	3	14	2	5
Salinity	32.8 ± 1.0	33.8 ± 0.2	33.9 ± 0.0	33.8 ± 0.2
T_w (°C)	18.2 ± 0.6	24.6 ± 2.5	24.4 ± 0.3	25.3 ± 0.8
$a_g(412)$ (m^{-1})	0.12 ± 0.04	0.04 ± 0.02	0.05 ± 0.01	0.06 ± 0.01
[N + N] (μM)	7.8 ± 5.5	0.2 ± 0.4	0.3 ± 0.2	0.2 ± 0.2
May to October – Southwest monsoon and inter-monsoonal periods				
Stations	28	14	5	71
Salinity	29.2 ± 6.6	33.3 ± 0.7	33.4 ± 1.2	33.6 ± 0.3
T_w (°C)	27.7 ± 1.6	28.3 ± 1.6	28.1 ± 1.7	28.6 ± 1.0
$a_g(412)$ (m^{-1})	0.16 ± 0.13	0.05 ± 0.02	0.05 ± 0.02	0.04 ± 0.01
[N + N] (μM)	16.1 ± 27.2	0.2 ± 0.4	0.2 ± 0.3	0.0 ± 0.0

* T_w: water temperature; $a_g(412)$: absorption coefficient of colored dissolved organic matter at 412 nm; [N + N]: concentration of [nitrite + nitrate].

October and they were associated with a lower salinity. These were consistent with the elevated influence of the discharge of Pearl River water to the NoSoCS in the summer months (Guo et al., 2008; Pan et al., 2015). In contrast, in the outer shelf and the open NSCS, while $a_g(412)$ and the concentrations of [N + N] were generally low, slightly higher values were found in November to April and they were accompanied by higher salinities and lower temperatures. These were indicative of the increased influence of convective vertical mixing under the strong northeast monsoon in the winter months (Pan et al., 2015; Tseng et al., 2005).

3.2. Development and validation of the algorithm for remotely sensed concentrations of [N + N]

3.2.1. Relationship between the concentration of [N + N] and SST

The relationship between the concentration of [N + N] and SST in the top 20 m of the mixed layer is shown in Fig. 2. For the data set as a whole, the correlation ($P = 0.435$) between the two was poor, indicating that the concentration of [N + N] in the NoSoCS could not be estimated from SST alone. When the data set was sub-divided according to the hydrographic sub-divisions and the monsoonal seasons, significant correlations were found in the open NSCS over the whole year ($P < 0.001$) and over all hydrographic sub-divisions during the northeast monsoonal season ($P < 0.001$) at SST below ~26 °C (Fig. 2, Table 2). At SST above ~26 °C, the concentration of [N + N] in the oceanic waters, < 0.1 μM, became undetectable. This threshold temperature is similar to that, 25–27 °C, reported previously in the open South China Sea (Kamykowski et al., 2002). In both cases, the negative correlation between the concentration of [N + N] and SST found in the open ocean was maintained probably because the contribution of [N + N] to the mixed layer by vertical mixing had dominated over that by riverine input. Thus, in the former case, the riverine influence is limited in the open NSCS. In the latter case, the riverine input reaches a minimum while vertical mixing becomes most effective during the drier northeast monsoonal season. Nevertheless, even in the latter case, the correlation ($r^2 = 0.605$) between the concentration of [N + N] and SST was only moderate as the $RMSE_{log}$ in log ([N + N]) and the MAPD in the concentration of [N + N] were both unacceptably large, reaching 0.451 and 172% respectively (Table 2). Thus, SST alone is not a viable proxy for the concentration of [N + N] in a river-influenced shelf-sea such as the NoSoCS.

3.2.2. CDOM as an indicator of the influence of riverine input

The relationship between $a_g(412)$ and salinity is shown in Fig. 3a. At salinities above ~33 in waters mostly seaward of the middle shelf,

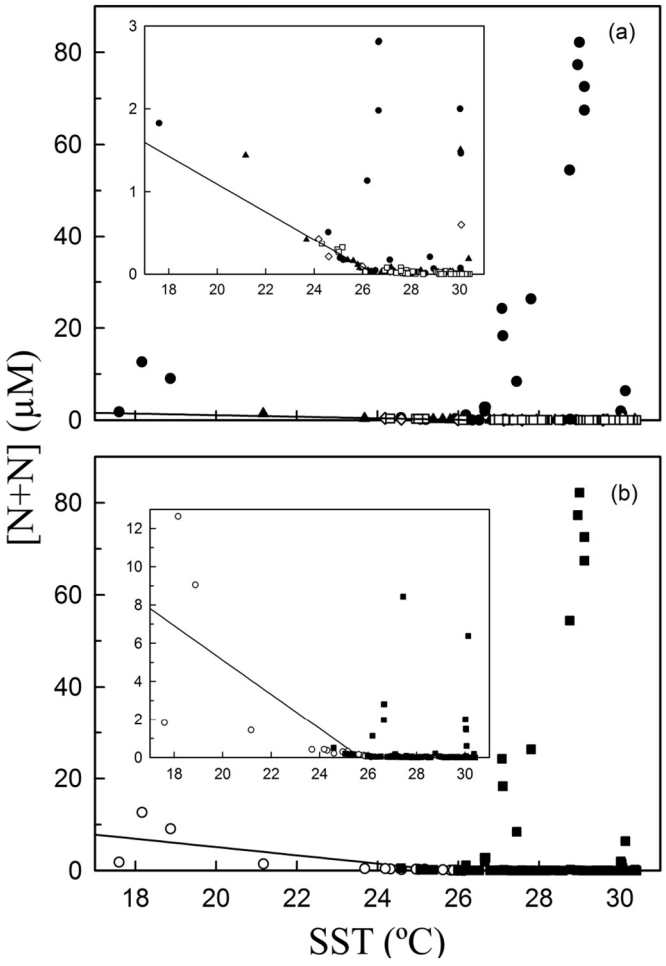

Fig. 2. The relationships between the concentration of [N + N] and SST in (a) the different hydrographic sub-divisions (● – inner shelf, ▲ – middle shelf, ◊ - outer shelf, □ – open NSCS) and (b) the different times of the year (○ – November–April, northeast monsoonal season; ■ – May–October). Expanded concentration scales are used and the best fit lines in the open NSCS and in November–April are shown in the insets.

$a_g(412)$ was weakly dependent to approximately independent of salinity. In lower salinity waters, which were found almost exclusively in the inner shelf where the riverine influence was the most extensive, $a_g(412)$ increased systematically with decreasing salinity and the relationship could be approximated well as a linear relationship such that:

$$a_g(412) = (0.692 \pm 0.041) - (0.0180 \pm 0.0014)\,\text{Salinity}$$
$$r^2 = 0.884,\ n = 25 \quad (5)$$

This relationship was not dependent on the time of the year as similar relationships with similarly high correlation coefficients could be found during the northeast monsoonal season and during the rest of the year. The strong negative correlation between $a_g(412)$ and salinity shows that $a_g(412)$ is a good indicator of the influence of the fresher riverine input in NoSoCS.

The relationship between the concentration of [N + N] and $a_g(412)$ is shown in Fig. 3b. At salinities below ~33 where $a_g(412)$ rose above ~0.1 m^{-1} (Fig. 3a), the concentration of [N + N] in these mostly inner shelf waters increased steadily with $a_g(412)$ and could be approximated well as a linear relationship such that:

$$[N + N] = (-20.3 \pm 5.6) + (220 \pm 24)[a_g(412)]$$
$$r^2 = 0.860,\ n = 16 \quad (6)$$

On the other hand, at lower $a_g(412)$ and higher salinities, < ~0.1 m^{-1} and > ~33 respectively, which were found in most of the NoSoCS

Table 2
Performance of the relationships between the concentration of [N + N] and SST in the different hydrographic sub-divisions and monsoonal seasons.

Sub-group	n	Best-fit relationships	r^2	$RMSE_{log}$	MAPD
All	142	n.s.	< 0.01	–	–
Inner shelf	31	n.s.	0.07	–	–
Middle shelf	28	n.s.	0.06	–	–
Outer shelf	7	n.s.	< 0.01	–	–
Open SCS	76	[N + N] = (4.45 ± 1.02) − (0.168 ± 0.041)[SST]	0.774	0.111	20%
Nov–Apr	25	[N + N] = (23.1 ± 3.7) − (0.899 ± 0.152)[SST]	0.605	0.451	172%
May–Oct	117	n. s.	< 0.01	–	–

n.s. – no significant correlation (P > 0.05); n – number of stations; $RMSE_{log}$ – root mean square error for log([N + N]); MAPD – mean absolute percentage difference for [N + N].

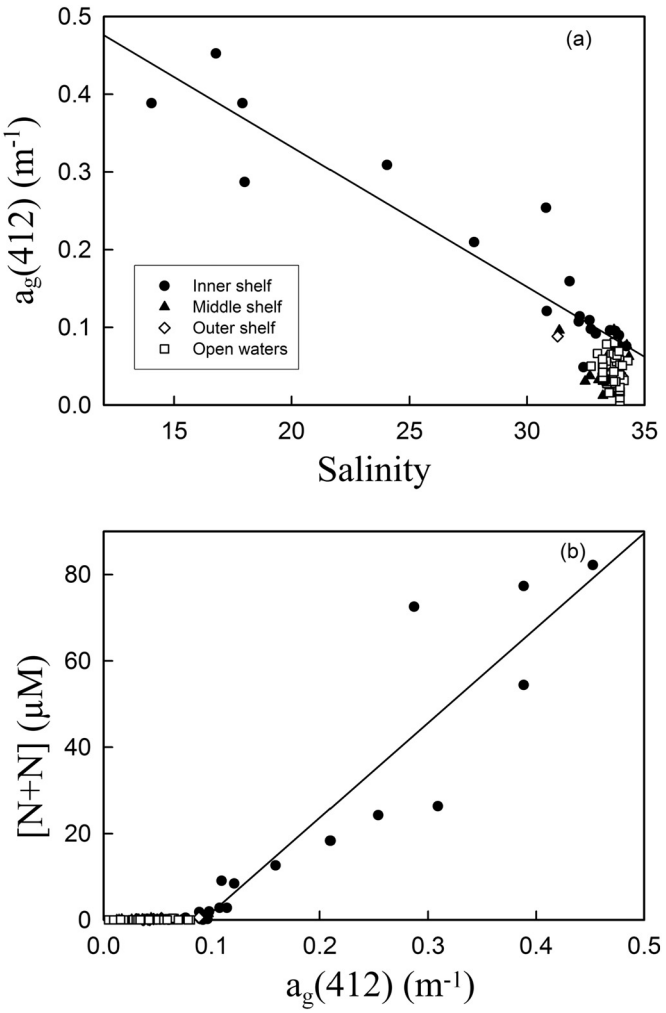

Fig. 3. The relationships between (a) $a_g(412)$ and salinity and (b) the concentration of [N + N] and $a_g(412)$. −− – best fits as in Eqs. (5) and (6).

and in the open NSCS, the concentration of [N + N] was not strongly correlated to $a_g(412)$ ($r^2 = 0.267$, $P < 0.001$). This poorer correlation was probably due to the limited riverine contribution in [N + N] and the higher uncertainties in the measurements of these lower $a_g(412)$ in these waters. Thus, $a_g(412)$ was a good proxy of [N + N] in the fresher waters where both the concentration of [N + N] and $a_g(412)$ were elevated.

3.2.3. Developing an algorithm for the concentration of [N + N] based on the combination of SST and $a_g(412)$

In developing the algorithm, characteristic values in SST and $a_g(412)$ were first established for evaluating the presence and absence of riverine [N + N] and [N + N] from vertical mixing. Based on these characteristic values in SST and $a_g(412)$ and the concentration of [N + N], the waters in the study area were subdivided into four types:

Type A: waters devoid of [N + N];
Type B: waters with [N + N] from riverine sources alone;
Type C: waters with [N + N] from vertical mixing alone;
Type D: waters with [N + N] from both sources.

Then, the relationship between the concentration of [N + N] and SST and/or $a_g(412)$ in each type of water was developed.

Samples with virtually no riverine [N + N], Type C waters, were identified from their location of collection (seaward of at least the inner shelf), their salinities (> ~33), and their $a_g(412)$ value (< ~0.1 m^{-1}) (Fig. 3). In these samples, [N + N] was supplied virtually exclusively by vertical mixing and the concentrations of [N + N] would be closely correlated to SST as widely reported in the open oceans (Kamykowski et al., 2002; Switzer et al., 2003). The relationship between the concentration of [N + N] and SST in these samples is shown in Fig. 4a. It followed a tightly defined curve which could be expressed as a 3rd-order polynomial function of SST. A regression analysis yielded a best-fit relationship such that:

$$[N + N]_{SST} = A_0 + A_1[SST] + A_2[SST]^2 + A_3[SST]^3$$
$$r^2 = 0.972,\ n = 106 \quad (7)$$

Here, $[N + N]_{SST}$ was the concentration of [N + N] in this type of water. The derived coefficients were: $A_0 = 69.00 \pm 3.89$, $A_1 = -7.078 \pm 0.448$, $A_2 = 0.2420 \pm 0.0171$, $A_3 = -0.002757 \pm 0.000217$. The coefficient of determination was remarkably high and the uncertainties in the derived coefficients, about ± 6 to 8%, were reasonably low, suggesting that the equation represented the relationship well. The equation indicates that $[N + N]_{SST}$ became zero when SST reached 31.4 °C. This temperature was then used for defining waters that were devoid of [N + N] from vertical mixing.

The concentration of riverine [N + N], $[N + N]_{CDOM}$, in the remaining samples was then calculated as the difference between the observed concentration of [N + N] and the concentration of [N + N] estimated by using Eq. (7). The relationship between $[N + N]_{CDOM}$ and $a_g(412)$ is shown in Fig. 4b. At $a_g(412)$ above ~0.1 m^{-1}, $[N + N]_{CDOM}$ was linearly related with $a_g(412)$ such that:

$$[N + N]_{CDOM} = B_0 + B_1[a_g(412)]$$
$$r^2 = 0.882,\ n = 20 \quad (8)$$

The derived coefficients were: $B_0 = -20.06 \pm 3.71$ and $B_1 = 218.3 \pm 17.9$. Again, the coefficient of determination was noticeably high and the uncertainties in the coefficient, 18% and 8%, were reasonably low. The equation indicates that $[N + N]_{CDOM}$ reached zero at $a_g(412)$ of 0.092 m^{-1}, which was then used as the criterion for defining the presence or the absence of riverine [N + N].

Based on these two criteria in $a_g(412)$ and SST, the four types of water were defined and the concentration of [N + N] in each of them was estimated as follows:

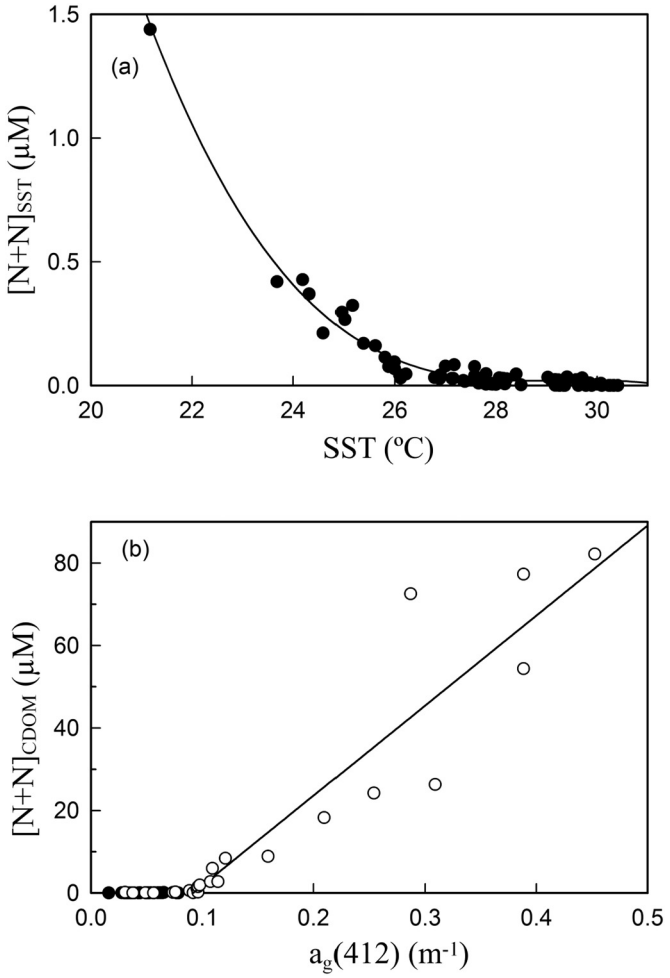

Fig. 4. The relationships between (a) $[N + N]_{SST}$ and SST and (b) $[N + N]_{CDOM}$ and $a_g(412)$. –– – best fits as in Eqs. (7) and (8).

Type A: SST > 31.4°C and $a_g(412) < 0.092\,m^{-1}$,

$$[N + N] = 0 \quad (9a)$$

Type B: SST > 31.4°C and $a_g(412) > 0.092\,m^{-1}$,

$$[N + N] = [N + N]_{CDOM} = -20.06 + 218.3[a_g(412)] \quad (9b)$$

Type C: SST < 31.4°C and $a_g(412) < 0.092\,m^{-1}$,

$$[N + N] = [N + N]_{SST} = 69.00 - 7.078[SST] + 0.2420[SST]^2 - 0.002757[SST]^3 \quad (9c)$$

Type D: SST < 31.4°C and $a_g(412) > 0.092\,m^{-1}$,

$$[N + N] = [N + N]_{SST} + [N + N]_{CDOM} = 48.94 - 7.078[SST] + 0.2420[SST]^2 - 0.002757[SST]^3 + 218.3[a_g(412)] \quad (9d)$$

The relationship between the observed and derived [N + N] is shown in Fig. 5. The $RMSE_{log}$ of log([N + N]) was 0.205, while the MAPD of [N + N] was 37.7%. In comparison, the corresponding values were 0.804 and 752% when the concentration of [N + N] was estimated from $a_g(412)$ alone, and indeterminate because of a lack of a statistical relationship when the concentration of [N + N] was estimated from SST alone. The reduction in $RMSE_{log}$ and MAPD in this new algorithm was dramatic. In fact, the MAPD was quite similar to that in the algorithms, ± 33% (Switzer et al., 2003), presently used in the estimation of the concentration of [N + N] in the major ocean basins from remotely sensed SST alone. This indicates that the surface concentration of [N + N] in the waters in the NoSoCS may be estimated

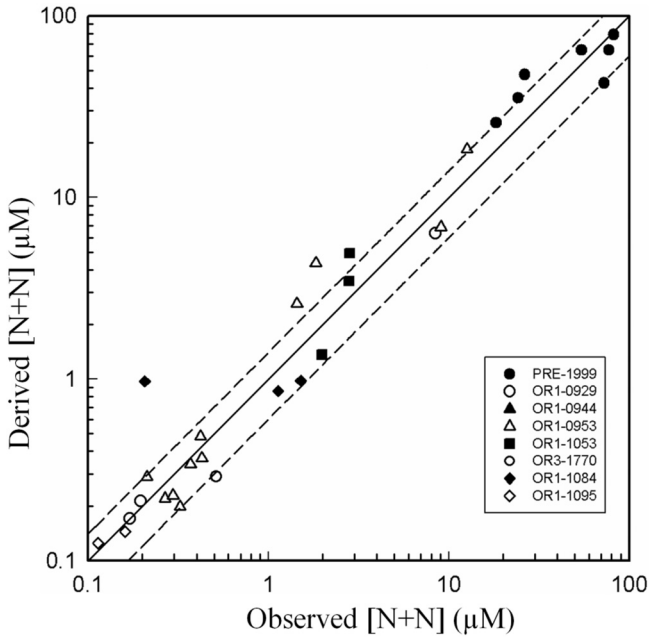

Fig. 5. The relationship between the derived and the observed concentrations of [N + N]. –– – 1:1 relationship; —— – ± 40% from the 1:1 line.

from the combination of $a_g(412)$ and SST at a similarly acceptable level of accuracy and precision as in the major ocean basins.

3.2.4. Validation of remotely sensed [N + N]

The performance of the proposed algorithm was further validated by comparing the concentration of [N + N] estimated from remotely sensed $a_g(412)$ and SST to those observed *in situ*, by following the protocols of Bailey and Werdell (2006). A wider satellite overpass time window of ± 24 h, rather than ± 3 h as proposed by Bailey and Werdell (2006), was allowed due to the paucity of remotely sensed data in the study area as a result of the frequent cloud cover. Using a wider time window would introduce additional uncertainty in the comparison as a result of a higher probability of temporal mismatches (Pan et al., 2008, 2010). Thus, the comparison might tend to underestimate the performance of the algorithm. The resulting $RMSE_{log}$ in log([N + N]) and MAPD in [N + N] were 0.224 and 40.2%, respectively (Fig. 6). These values were slightly larger but still quite comparable to those found in the algorithm development, 0.205 and 37.7%, suggesting that there was a reasonable agreement between the remotely sensed and the observed concentration of [N + N], especially in view of the wide time window that was used in the comparison. Nevertheless, since only 16 match-up data points were available for this evaluation, further validation when additional field observations became available would be desirable.

7In this study, $a_g(412)$ derived from a global, rather than a regionally tuned, algorithm was used for estimating [N + N]. Since the former is likely to be less reliable than the latter, this source of additional imprecision would propagate into the estimated [N + N] in Type B (Eq. (9b)) and Type D (Eq. (9d)) waters. These waters were found primarily in the inner shelf, which covers about 40% of the area of the NoSoCS (Wong et al., 2015b). The occurrence of Type B water was further limited only to the summer at the very mouth of the Pearl River where both SST, > 31.4 °C, and $a_g(412)$, > $0.092\,m^{-1}$, could be elevated. Due to the lack of regional data, it is presently not possible to evaluate the exact magnitude of this source of error in the NoSoCS. However, in the southern Middle Atlantic Bight, $a_g(412)$ derived from a regionally tuned algorithm have been reported previously (Pan et al., 2008) and the corresponding $a_g(412)$ derived from the global algorithm were obtained by re-processing the data using Eq. (2) (Pan, unpublished data). The average % deviations from the observed values in $a_g(412)$ derived from a global and a

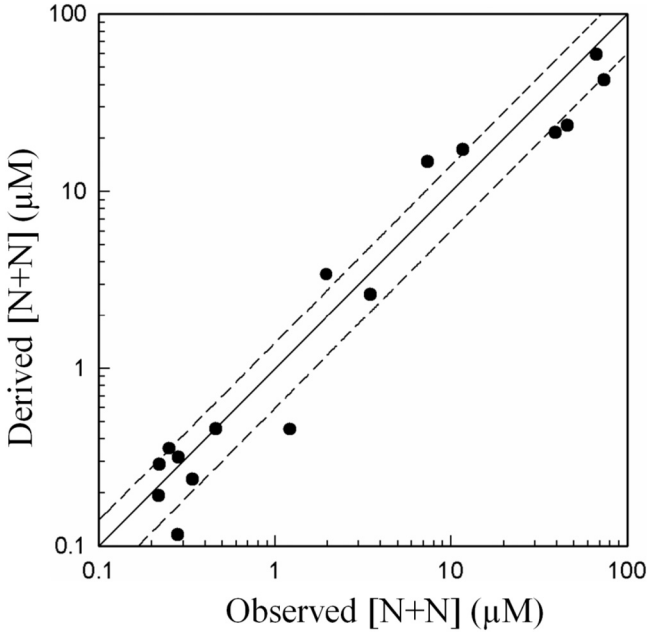

Fig. 6. The relationship between the satellite-derived and observed concentrations of [N + N] matched within a ± 24 hour time window. −− – 1:1 relationship; —— – ± 40% from the 1:1 line.

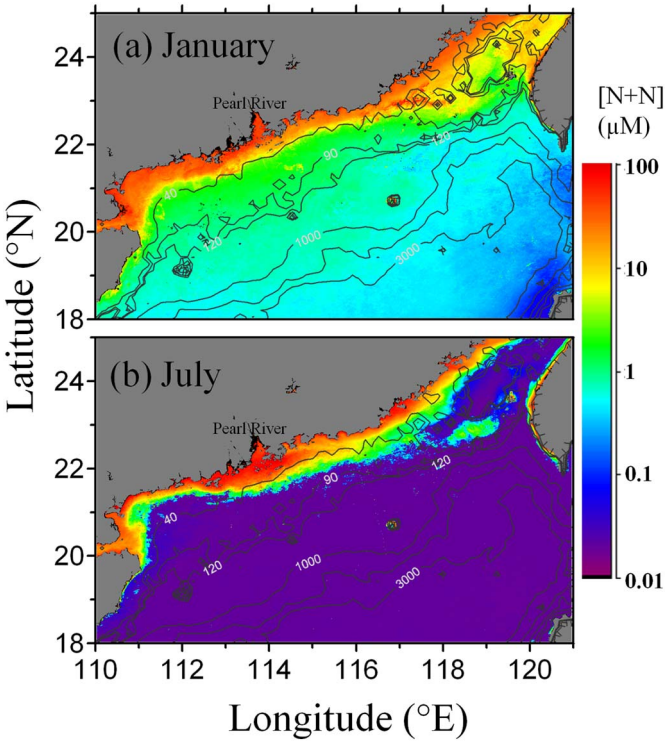

Fig. 7. The climatological (2002–2014) monthly average distributions of the concentrations of [N + N] by MODIS-Aqua in the NoSoCS and adjacent waters in (a) January and (b) July.

regionally tuned algorithm were about ± 40% and ± 20%, respectively. The % deviation of the former relative to the latter varied between about −40% and +50% in a range of $a_g(412)$ of 0.05 to 0.35 m^{-1}. The corresponding MAPD was about ± 30%. Both the uncertainty in $a_g(412)$ derived from a global algorithm and the range of $a_g(412)$ in the southern Middle Atlantic Bight were similar to those found in the NoSoCS. If the estimated $a_g(412)$ in the NoSoCS by using the two algorithms followed the same pattern as that in the southern Middle Atlantic Bight, the $RMSE_{log}$ and MAPD in the [N + N] derived from a global algorithm as shown (Fig. 6) would represent a high estimate which can be improved when a regionally tuned algorithm becomes available for use. Furthermore, when an error in $a_g(412)$ of ± 30% and ± 40% is applied to impose on the [N + N] derived from a global algorithm, the MAPD was increased only moderately from ± 40% as in Fig. 6 to ± 50% and ± 60%, respectively. Thus, while a regional tuning of the algorithm for $a_g(412)$ will likely reduce the uncertainty in the estimated [N + N], it is unlikely to invalidate the general relationships and the distributional patterns in [N + N] reported here.

3.3. The climatological distribution of remotely sensed [N + N] in the NoSoCS and adjacent waters

The climatological monthly average distribution of the remotely sensed concentration of [N + N] in January and July during the northeast and the southwest monsoonal season respectively in the NoSoCS and adjacent waters are shown in Fig. 7.

In both months, there is a general trend of increasing [N + N] towards the coast, varying typically over two orders of magnitude from < 0.5 μM and near zero in the open NSCS in January and July respectively to about 50 μM and 100 μM at the mouth of the Pearl River, consistent with the reports based on direct observations (Chen et al., 2004a; Wong et al., 2015a; Yin, 2002). The Pearl River plume, indicated by the elevated concentrations (> 50 μM) at the mouth of the River, is small and is confined only to a narrow band along the coast west of the river mouth in January but it is more extensive in July as it spreads northeastward into the middle shelf. These patterns are consistent with the effects of the lower flow from the River coupled with the prevailing northeast monsoonal wind in January and the higher flow from the River together with the prevailing southwest monsoonal wind in July (Gan et al., 2009, 2010; Pan et al., 2015). A patch of waters with elevated concentrations of [N + N], around 1 μM, was found off the southwestern edge of the Taiwan Bank, in which water depths are 20 to 40 m (Yang et al., 2010), in July in the midst of waters that are almost devoid of [N + N]. Since the $a_g(412)$ in this general location has been reported to be < 0.1 m^{-1} (Dong et al., 2013), it would have been disregarded in the algorithm in the estimation of the concentration of [N + N] so that the elevated concentrations found was driven by a depression in SST alone (Eq. (9c)). Thus, this pattern in [N + N] is consistent with the summer upwelling, which has been reported to bring colder and more [N + N]-replete water to the sea surface in this general area (Hong et al., 2011; Huang et al., 2011).

The intra-annual variations in the satellite-derived monthly average concentration of [N + N] and SST in the NoSoCS as a whole and in the different hydrographic sub-regions in the study area are shown in Fig. 8. The range of concentrations in each case compares reasonably well with the corresponding values found in direct observations (Table 1). In the open NSCS, the intra-annual variations in the monthly average concentration of [N + N] follow a distinct seasonal cycle, dropping to a minimum at near zero in July–August and rising to a maximum of ~ 0.7 μM in January. The monthly average concentration of [N + N] is strongly negatively correlated with the monthly average SST ($r = -0.90$), confirming that the enhanced vertical convective mixing in the winter by surface cooling and the stronger wind is a primary control of the surface concentration of [N + N] in the open NSCS (Tseng et al., 2005). In the NoSoCS, in addition to the primary maximum in the winter, a secondary summer maximum in the concentration of [N + N] can also be found. This secondary maximum becomes increasingly prominent towards the coast and this is consistent with the influence of the riverine input of [N + N] to the NoSoCS which reaches a maximum in the summer (Yin, 2002). As a result of this additional source of [N + N] to the NoSoCS, the monthly average concentration in [N + N] is not well correlated with that in SST in the NoSoCS ($r = -0.20$). In fact, the correlation becomes weaker shoreward and is insignificant in the inner shelf.

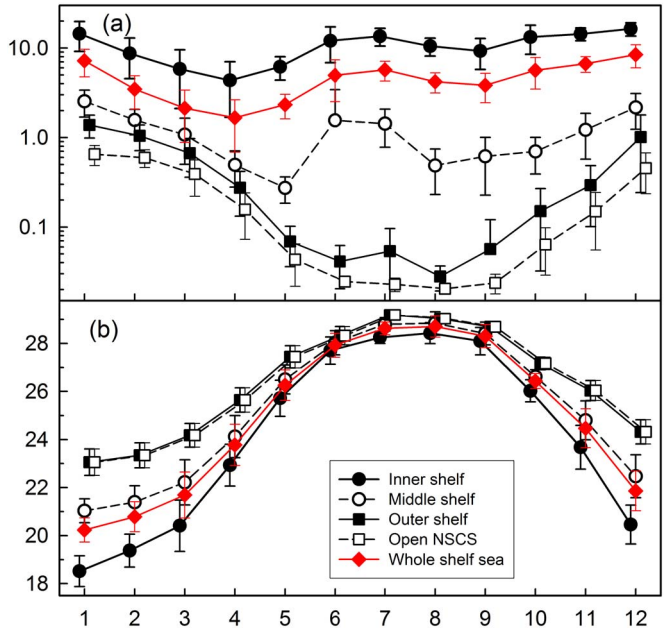

Fig. 8. The climatological (2002–2014) monthly averages in (a) the concentration of [N + N] and (b) SST by MODIS-Aqua in the different hydrographic sub-divisions in the NoSoCS and the adjacent open NSCS. Error bar – 1 SD from each average value.

3.4. Applicability to other river-influenced shelf-seas – the Texas-Louisiana Shelf in the northern Gulf of Mexico

As the receiving water of the Mississippi River, the Texas-Louisiana Shelf in the northern Gulf of Mexico off the coasts of the southern United States, is also a river-influenced shelf-sea (Cai, 2003; Del Castillo and Miller, 2008; Huang et al., 2015) like the NoSoCS. When the data in [N + N], SST and $a_g(412)$ from the Texas-Louisiana Shelf were treated similarly as those from the NoSoCS, similar patterns in the relationships between $[N + N]_{SST}$ and SST and between $[N + N]_{CDOM}$ and $a_g(412)$ were found (Fig. 9). Although the data-set was not extensive enough for a quantitative statistical analysis, $[N + N]_{SST}$, which was the [N + N] in waters with salinities above ~35 and water depths exceeding ~40 m, generally decreased with increasing SST until it reached a nitrate-depletion temperature, about 28 °C in this case (Fig. 9a). On the other hand, $[N + N]_{CDOM}$, which was the [N + N] in waters with salinities below 33, increased systematically with increasing $a_g(412)$ (Fig. 9b). The relationship was approximately linear such that:

$$[N + N]_{CDOM} = (-12.6 \pm 5.3) + (45.6 \pm 3.9)[a_g(412)]$$
$$r^2 = 0.918,\ n = 12 \qquad (10)$$

As indicated by the high r^2 in the relationship, $[N + N]_{CDOM}$ in the Texas-Louisiana Shelf was strongly correlated to $a_g(412)$ as in the NoSoCS. Although the present data set was not sufficiently extensive for deriving the relationship between [N + N] and the combination of SST and $a_g(412)$, these two relationships do indicate the strong likelihood that [N + N] may be parameterized by them so that [N + N] may be similarly assessed by remote sensing in the Texas-Louisiana Shelf, and possibly even in other river-influenced shelf-seas, as in the NoSoCS. It should be noted that, while the general trends were similar, the relationships between $[N + N]_{SST}$ and SST and between $[N + N]_{CDOM}$ and $a_g(412)$ in the Texas-Louisiana Shelf and the NoSoCS were quantitatively different so that the best fit lines in the latter could not represent the observations in the former well (Fig. 9). Thus, an empirical regional tuning will be necessary if [N + N] in the river-influenced shelf-seas is to be assessed from remotely sensed SST and $a_g(412)$.

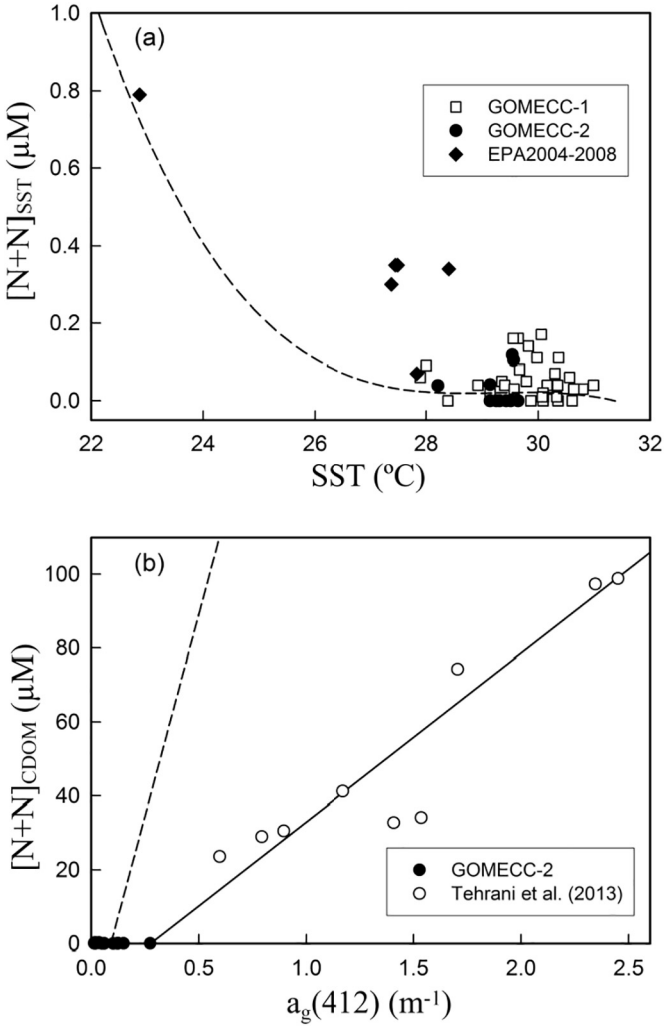

Fig. 9. Same to Fig. 4 but for the Texas-Louisiana Shelf in the northern Gulf of Mexico. Solid line – best fit for the Texas-Louisiana Shelf; dashed lines – best fits for the NoSoCS as in Fig. 4.

4. Conclusions

This study has demonstrated that, by including an ocean color component in the algorithm, the surface concentration of [N + N] in the NoSoCS and adjacent waters, where the influence of riverine input is significant, may be assessed from space by using remotely sensed SST and CDOM absorption together. The uncertainty in the remotely sensed concentration of [N + N] is about ± 40%.

The spatial and temporal distributional patterns in the remotely sensed monthly average concentration of [N + N] in the NoSoCS and its adjacent waters are consistent with those derived from *in situ* observations. The concentration of [N + N] generally increases landward in response to the increasing riverine influence. In the open NSCS, a prominent maximum in the concentration of [N + N] is found in the winter and the monthly average concentration of [N + N] is strongly negatively correlated with that of SST as a result of the effect of the enhanced vertical convective mixing in the winter. Pearl River water is elevated in the concentration of [N + N] and the Pearl River plume in the NoSoCS can be clearly depicted by this property. Because of the strong riverine influence in the NoSoCS, in addition to the primary winter maximum, a secondary maximum in the concentration of [N + N] can also be found in the NoSoCS in the summer when the river-runoff reaches its peak and this summer maximum becomes increasingly prominent towards the coasts. Higher concentrations of [N + N]

are also found in the summer off the southwest edge of the Taiwan Bank where upwelling is known to occur.

Similar patterns in the relationships between [N + N] and SST and between [N + N] and $a_g(412)$ may also be found in other river-influenced shelf-seas, such as the Texas-Louisiana Shelf, suggesting that [N + N] may be similarly assessed by remote sensing in these shelf waters. However, an empirical regional tuning will be necessary as the relationships may differ quantitatively from region to region.

Acknowledgements

K.-Y. Li, Y.-C. Wu, H.-H. Yang, L.-T. Hou, W.-C. Tu and the captains and crews of R/V *Ocean Researcher I* and R/V *Ocean Researcher III* assisted in sample collection and/or sample analyses. This work was supported in part by the National Natural Science Foundation of China (grant No. 41630966), the Scientific and Technological Innovation Project of the Qingdao National Laboratory for Marine Science and Technology (grant No. 2016ASKJ02), the Key Research and Development Program of Shandong Province (grant No. 2015GSF117017), and Ocean University of China (grant No. 201513037 and 201512011) to Pan, and by the Ministry of Science and Technology, Taiwan (grant Nos. NSC98-2611-M-001-004-MY3 and NSC100-2611-M-001-001) and the Academia Sinica through grants titled "Atmospheric Forcing on Ocean Biogeochemistry (AFOBi)" and "Ocean Acidification: Comparative biogeochemistry in shallow-water tropical coral reef ecosystems in a naturally acidic marine environment" to Wong. The preparation of this manuscript was completed while Wong was supported as a visiting professor at the MCTL, Ocean University of China. This is MCTL Contribution No. 129.

References

Arteaga, L., Pahlow, M., Oschlies, A., 2015. Global monthly sea surface nitrate fields estimated from remotely sensed sea surface temperature, chlorophyll, and modeled mixed layer depth. Geophys. Res. Lett. 42, 1130–1138. http://dx.doi.org/10.1002/2014GL062937.

Bai, Y., Pan, D., Cai, W.-J., He, X., Wang, D., Tao, B., Zhu, Q., 2013. Remote sensing of salinity from satellite-derived CDOM in the Changjiang River dominated East China Sea. J. Geophys. Res. 118, 227–243. http://dx.doi.org/10.1029/2012JC008467.

Bailey, S.W., Werdell, P.J., 2006. A multi-sensor approach for the on-orbit validation of ocean color satellite data products. Remote Sens. Environ. 102, 12–23. http://dx.doi.org/10.1016/j.rse.2006.01.015.

Bonsdorff, E., Blomqvist, E.M., Mattila, J., Norkko, A., 1997. Coastal eutrophication: causes, consequences and perspectives in the Archipelago Areas of the Northern Baltic Sea. Estuar. Coast. Shelf Sci. 44, 63–72.

Cai, W.-J., 2003. Riverine inorganic carbon flux and rate of biological uptake in the Mississippi River plume. Geophys. Res. Lett. 30, 1032.

Cai, W.-J., 2011. Estuarine and coastal ocean carbon paradox: CO_2 sinks or sites of terrestrial carbon incineration? Annu. Rev. Mar. Sci. 3, 123–145. http://dx.doi.org/10.1146/annurev-marine-120709-142723.

Cai, W.-J., Dai, M., 2004. Comment on "Enhanced open ocean storage of CO_2 from shelf sea pumping". Science 306 (5701), 1477. http://dx.doi.org/10.1126/science.1102132.

Cai, W.-J., Dai, M., Wang, Y., Zhai, W., Huang, T., Chen, S., et al., 2004. The biogeochemistry of inorganic carbon and nutrients in the Pearl River estuary and the adjacent Northern South China Sea. Cont. Shelf Res. 24, 1301–1319. http://dx.doi.org/10.1016/j.csr.2004.04.005.

Cai, W.-J., Chen, C.-T.A., Borges, A.V., 2014. Carbon dioxide dynamics and fluxes in coastal waters influenced by river plumes. In: Bianchi, T.S., Allison, M.A., Cai, W.-J. (Eds.), Biogeochemical Dynamics at Major River-coastal Interfaces: Linkages With Global Change. Cambridge University Press, NY.

Callahan, J., Dai, M., Chen, R.F., Li, X.L., Lu, Z.M., Huang, W., 2004. Distribution of dissolved organic matter in the Pearl River Estuary, China. Mar. Chem. 89, 211–224. http://dx.doi.org/10.1016/j.marchem.2004.02.013.

Chen, C.-T.A., 2003. New vs. export production on the continental shelf. Deep-Sea Res. II 50, 1327–1333. http://dx.doi.org/10.1016/S0967-0645(03)00026-2.

Chen, J., Li, Y., Yin, K., Jin, H., 2004a. Amino acids in the Pearl River Estuary and adjacent waters: origins, transformation and degradation. Cont. Shelf Res. 24, 1877–1894. http://dx.doi.org/10.1016/j.csr.2004.06.013.

Chen, Z., Li, Y., Pan, J., 2004b. Distributions of colored dissolved organic matter and dissolved organic carbon in the Pearl River Estuary, China. Cont. Shelf Res. 24, 1845–1856. http://dx.doi.org/10.1016/j.csr.2004.06.011.

Chen, B., Zheng, L., Huang, B., Song, S., Liu, H., 2013. Seasonal and spatial comparisons of phytoplankton growth and mortality rates due to microzooplankton grazing in the northern South China Sea. Biogeosciences 10, 2775–2785. http://dx.doi.org/10.5194/bg-10-2775-2013.

Chou, W.-C., Tishchenko, P.Y., Chuang, K.-Y., Gong, G.-C., Shkirnikova, E.M., Tishchenko, P.P., 2017. The contrasting behaviors of CO_2 systems in river-dominated and ocean-dominated continental shelves: a case study in the East China Sea and the Peter the Great Bay of the Japan/East Sea in summer 2014. Mar. Chem. 195, 50–60. http://dx.doi.org/10.1016/j.marchem.2017.04.005.T.

Del Castillo, C.E., Miller, R.L., 2008. On the use of ocean color remote sensing to measure the transport of dissolved organic carbon by the Mississippi River Plume. Remote Sens. Environ. 112, 836–844. http://dx.doi.org/10.1016/j.rse.2007.06.015.

Dong, Q., Shang, S., Lee, Z., 2013. An algorithm to retrieve absorption coefficient of chromophoric dissolved organic matter from ocean color. Remote Sens. Environ. 128, 259–267. http://dx.doi.org/10.1016/j.rse.2012.10.013.

Gan, J., Cheung, A., Guo, X., Li, L., 2009. Intensified upwelling over a widened shelf in the northeastern South China Sea. J. Geophys. Res. 114, C09019. http://dx.doi.org/10.1029/2007JC004660.

Gan, J., Lu, Z., Dai, M., Cheung, A.Y.Y., Liu, H., Harrison, P., 2010. Biological response to intensified upwelling and to a river plume in the northeastern South China Sea: a modeling study. J. Geophys. Res. 115, C09001. http://dx.doi.org/10.1029/2009JC005569.

Gilbert, P.M., Maranger, R., Sobota, D.J., Bouwman, L., 2014. The Haber Bosch–harmful algal bloom (HB–HAB) link. Environ. Res. Lett. 9, 105001. http://dx.doi.org/10.1088/1748-9326/9/10/105001.

Goes, J.I., Saino, T., Oaku, H., Ishizaka, J., Wong, C.S., Nojiri, Y., 2000. Basin scale estimates of sea surface nitrate and new production from remotely sensed sea surface temperature and chlorophyll. Geophys. Res. Lett. 27, 1263–1266.

Guo, X., Cai, W.-J., Zhai, W., Dai, M., Wang, Y., Chen, B., 2008. Seasonal variations in the inorganic carbon system in the Pearl River (Zhujiang) estuary. Cont. Shelf Res. 28, 1424–1434. http://dx.doi.org/10.1016/j.csr.2007.07.011.

Hecky, R.E., Kilham, P., 1988. Nutrient limitation of phytoplankton in freshwater and marine environments: a review of recent evidence on the effects of enrichment. Limnol. Oceanogr. 33 (4, part 2), 196–822.

Ho, T.-Y., Pan, X., Yang, H.-H., Wong, G.T.F., Shiah, F.-K., 2015. Controls on temporal and spatial variations of phytoplankton pigment distribution in the northern South China Sea. Deep-Sea Res. II 117, 65–85. http://dx.doi.org/10.1016/j.dsr2.2015.05.015.

Hong, H., Liu, X., Chiang, K.-P., Huang, B., Zhang, C., Hu, J., Li, Y., 2011. The coupling of temporal and spatial variations of chlorophyll a concentration and the East Asian monsoons in the southern Taiwan Strait. Cont. Shelf Res. 31, S37–S47. http://dx.doi.org/10.1016/j.csr.2011.02.004.

Hu, J., Kawamura, H., Li, C., Hong, H., Jiang, Y., 2010. Review on current and seawater volume transport through the Taiwan Strait. J. Oceanogr. 66 (5), 591–610. http://dx.doi.org/10.1007/s10872-010-0049-1.

Huang, B., Xiang, W., Zeng, X., Chiang, K.-P., Tian, H., Hu, J., Lan, W., Hong, H., 2011. Phytoplankton growth and microzooplankton grazing in a subtropical coastal upwelling system in the Taiwan Strait. Cont. Shelf Res. 31, S48–S56. http://dx.doi.org/10.1016/j.csr.2011.02.005.

Huang, W.-J., Cai, W.-J., Wang, Y., Lohrenz, S.E., Murrell, M.C., 2015. The carbon dioxide system on the Mississippi River-dominated continental shelf in the northern Gulf of Mexico: 1. Distribution and air-sea CO_2 flux. J. Geophys. Res. 120, 1429–1445. http://dx.doi.org/10.1002/2014JC010498.

Hutahaean, A.A., Ishizaka, J., Morimoto, A., Kanda, J., Horimoto, N., Saino, T., 2010. Development of algorithms for estimating the seasonal nitrate profiles in the upper water column of the Sagami Bay, Japan. Lamer 48, 71–86.

JGOFS, 1994. Protocols for the Joint Global Ocean Flux Study (JGOFS) Core Measurements. JGOFS Report #19. UNESCO.

Kamykowski, D., Zentara, S.-J., Morrison, J.M., Switzer, A.C., 2002. Dynamic global patterns of nitrate, phosphate, silicate, and iron availability and phytoplankton community composition from remote sensing data. Glob. Biogeochem. Cycles 16 (4), 1077. http://dx.doi.org/10.1029/2001GB001640.

Levitus, S., Boyer, T.P., Garcia, H.E., Locarnini, R.A., Zweng, M.M., Mishonov, A.V., et al., 2014. World Ocean Atlas 2013 (NCEI Accession 0114815). Version 3.3. NOAA National Centers for Environmental Informationhttp://dx.doi.org/10.7289/V5F769GT.

Li, J., Glibert, P.M., Gao, Y., 2015. Temporal and spatial changes in Chesapeake Bay water quality and relationships to Prorocentrum minimum, *Karlodinium veneficum*, and CyanoHAB events, 1991–2008. Harmful Algae 42, 1–14. http://dx.doi.org/10.1016/j.hal.2014.11.003.

Liu, K.K., Chao, S.-Y., Shaw, P.-T., Gong, G.-C., Chen, C.-C., Tang, T.-Y., 2002. Monsoon-forced chlorophyll distribution and primary production in the South China Sea: observations and a numerical study. Deep-Sea Res. I 49, 1387–1412.

Liu, Q., Dai, M., Chen, W., Huh, C.-A., Wang, G., Li, Q., Charette, M.A., 2012. How significant is submarine groundwater discharge and its associated dissolved inorganic carbon in a river-dominated shelf system? Biogeosciences 9, 1777–1795.

Liu, K.-K., Wang, L.-W., Dai, M., Tseng, C.-M., Yang, Y., Sui, C.-H., et al., 2013. Interannual variation of chlorophyll in the northern South China Sea observed at the SEATS Station and its asymmetric responses to climate oscillation. Biogeosciences 10, 7449–7462. http://dx.doi.org/10.5194/bg-10-7449-2013.

Lohrenz, S.E., Cai, W.-J., Chakraborty, S., Gundersen, K., Murrell, M.C., 2014. Nutrient and carbon dynamics in a large river-dominated coastal ecosystem: the Mississippi-Atchafalaya River system. In: Bianchi, T.S., Allison, M.A., Cai, W.-J. (Eds.), Biogeochemical Dynamics at Major River-coastal Interfaces: Linkages With Global Change. Cambridge University Press, NY.

Mannino, A., Russ, M.E., Hooker, S.B., 2008. Algorithm development and validation for satellite-derived distributions of DOC and CDOM in the U.S. Middle Atlantic Bight. J. Geophys. Res. 113, C07051. http://dx.doi.org/10.1029/2007JC004493.

Mannino, A., Novak, M.G., Hooker, S.B., Hyde, K., Aurin, D., 2014. Algorithm development and validation of CDOM properties for estuarine and continental shelf waters along the northeastern U.S. coast. Remote Sens. Environ. 152, 576–602. http://dx.

doi.org/10.1016/j.rse.2014.06.027.
Mitchell, B.G., Kahru, M., Wieland, J., Stramska, M., 2002. Determination of spectral absorption coefficients of particles, dissolved material and phytoplankton for discrete water samples. In: Mueller, J.L., Fargion, G.S. (Eds.), Ocean Optics Protocols for Satellite Ocean Color Sensor Validation, Revision 3. Rep. NASA/TM-2002-210001/Rev3-Vol2, vol. 2. NASA Goddard Space Flight Center, Greenbelt, Maryland, pp. 231–257.
Moore, C.M., Mills, M.M., Arrigo, K.R., Berman-Frank, I., Bopp, L., Boyd, P.W., et al., 2013. Processes and patterns of oceanic nutrient limitation. Nat. Geosci. 6, 701–710. http://dx.doi.org/10.1038/ngeo1765.
O'Reilly, J.E., Maritorena, S., Mitchel, B.G., Siege, D.A., Carder, K.L., Garver, S.A., et al., 1998. Ocean color chlorophyll algorithms for SeaWiFS. J. Geophys. Res. 103, 24937–24953. http://dx.doi.org/10.1029/98JC02160.
Pai, S.-C., Yang, C.-C., Riley, J.P., 1990. Formation kinetics of the pink azo dye in the determination of nitrite in natural waters. Anal. Chim. Acta 232, 345–349.
Pan, X., Wong, G.T.F., 2015. An improved algorithm for remotely sensing marine dissolved organic carbon: climatology in the northern South China Sea Shelf-sea and adjacent waters. Deep-Sea Res. II 117, 131–142. http://dx.doi.org/10.1016/j.dsr2.2015.02.025.
Pan, X., Mannino, A., Russ, M.E., Hooker, S.B., 2008. Remote sensing of the absorption coefficients and chlorophyll a concentration in the United States southern Middle Atlantic Bight from SeaWiFS and MODIS-Aqua. J. Geophys. Res. 113, C11022. http://dx.doi.org/10.1029/2008JC004852.
Pan, X., Mannino, A., Russ, M.E., Hooker, S.B., Harding, L.W., 2010. Remote sensing of phytoplankton pigment distribution in the United States northeast coast. Remote Sens. Environ. 114, 2403–2416. http://dx.doi.org/10.1016/j.rse.2010.05.015.
Pan, X., Wong, G.T.F., Tai, J.-H., Ho, T.-Y., 2015. Climatology of physical hydrographic and biological characteristics of the northern South China Sea Shelf-sea (NoSoCS) and adjacent waters: observations from satellite remote sensing. Deep-Sea Res. II 117, 10–22. http://dx.doi.org/10.1016/j.dsr2.2015.02.022.
Pauly, D., Christensen, V., 1995. Primary production required to sustain global fisheries. Nature 374, 255–257.
Rabouille, C., Conley, D.J., Dai, M.H., Cai, W.-J., Chen, C.T.A., Lansard, B., Green, R., Yin, K., Harrison, P.J., Dagg, M., McKee, B., 2008. Comparison of hypoxia among four river-dominated ocean margins: the Changjiang (Yangtze), Mississippi, Pearl, and Rhône rivers. Cont. Shelf Res. 28, 1527–1537.
Rousseaux, C.S., Gregg, W.W., 2015. Recent decadal trends in global phytoplankton composition. Glob. Biogeochem. Cycles 29, 1674–1688. http://dx.doi.org/10.1002/2015GB005139.
Silió-Calzada, A., Bricaud, A., Gentili, B., 2008. Estimates of sea surface nitrate concentrations from sea surface temperature and chlorophyll concentration in upwelling areas: a case study for the Benguela system. Remote Sens. Environ. 112, 3173–3180. http://dx.doi.org/10.1016/j.rse.2008.03.014.
Strickland, J.D.H., Parsons, T.R., 1972. A Practical Handbook of Seawater Analysis, Bulletin 167, 2nd edition. Fisheries Research Board of Canada, Ottawa.
Strokal, M., Yang, H., Zhang, Y., Kroeze, C., Li, L., Luan, S., et al., 2014. Increasing eutrophication in the coastal seas of China from 1970 to 2050. Mar. Pollut. Bull. 85, 123–140. http://dx.doi.org/10.1016/j.marpolbul.2014.06.01.
Switzer, A.C., Kamykowski, D., Zentara, S.-J., 2003. Mapping nitrate in the global ocean using remotely sensed sea surface temperature. J. Geophys. Res. 108 (C8), 3280. http://dx.doi.org/10.1029/2000JC000444.
Tehrani, N.C., D'Sa, E.J., Osburn, C.L., Bianchi, T.S., Schaeffer, B.A., 2013. Chromophoric dissolved organic matter and dissolved organic carbon from sea-viewing wide field-of-view sensor (SeaWiFS), moderate resolution imaging spectroradiometer (MODIS) and MERIS sensors: case study for the Northern Gulf of Mexico. Remote Sens. 5, 1439–1464. http://dx.doi.org/10.3390/rs5031439.
Thomas, H., Bozec, Y., Elkalay, K., de Baar, H.J.W., 2004. Enhanced open ocean storage of CO_2 from shelf sea pumping. Science 304 (5673), 1005–1008. http://dx.doi.org/10.1126/science.1095491.
Tseng, C.-M., Wong, G.T.F., Lin, I.-I., Wu, C.-R., Liu, K.-K., 2005. A unique seasonal pattern in phytoplankton biomass in low-latitude waters in the South China Sea. Geophys. Res. Lett. 32, L08608. http://dx.doi.org/10.1029/2004GL022111.
Wakelin, S.L., Artioli, Y., Butenschön, M., Allen, J.I., Holt, J.T., 2015. Modelling the combined impacts of climate change and direct anthropogenic drivers on the ecosystem of the northwest European continental shelf. J. Mar. Syst. 152, 51–63. http://dx.doi.org/10.1016/j.jmarsys.2015.07.006.
Wang, J., Hong, H., Jiang, Y., Chai, F., Yan, X.-H., 2013. Summer nitrogenous nutrient transport and its fate in the Taiwan Strait: a coupled physical–biological modeling approach. J. Geophys. Res. 118, 4184–4200.
Wei, J., Lee, Z., Shang, S., 2016. A system to measure the data quality of spectral remote-sensing reflectance of aquatic environments. J. Geophys. Res. 121, 8189–8207. http://dx.doi.org/10.1002/2016JC012126.
Wong, G.T.F., Tseng, C.-M., Wen, L.-S., Chung, S.-W., 2007. Nutrient dynamics and N-anomaly at the SEATS station. Deep-Sea Res. II 54, 1528–1545. http://dx.doi.org/10.1016/j.dsr2.2007.05.011.
Wong, G.T.F., Pan, X., Li, K.-Y., Shiah, F.-K., Ho, T.-Y., Guo, X., 2015a. Hydrography and nutrient dynamics in the Northern South China Sea Shelf-sea (NoSoCS). Deep-Sea Res. II 117, 23–40. http://dx.doi.org/10.1016/j.dsr2.2015.02.023.
Wong, G.T.F., Ku, T.-L., Liu, H., Mulholland, M., 2015b. The oceanography of the Northern South China Sea Shelf-sea (NoSoCS) and its adjacent waters – overview and highlights. Deep-Sea Res. II 117, 3–9. http://dx.doi.org/10.1016/j.dsr2.2015.04.026.
Yang, J., Zhang, J., Meng, J., 2010. Underwater topography detection of Taiwan Shoal with SAR images. Chin. J. Oceanol. Limnol. 28 (3), 636–642. http://dx.doi.org/10.1007/s00343-010-9070-x.
Yin, K., 2002. Monsoonal influence on seasonal variations in nutrients and phytoplankton biomass in coastal waters of Hong Kong in the vicinity of the Pearl River estuary. Mar. Ecol. Prog. Ser. 245, 111–122.
Yin, K., Xu, J., Lai, Z., Harrison, P.J., 2014. Dynamics of phytoplankton blooms and nutrient limitation in the Pearl River (Zhujiang) estuarine coastal waters. In: Bianchi, T.S., Allison, M.A., Cai, W.-J. (Eds.), Biogeochemical Dynamics at Major River-coastal Interfaces: Linkages with Global Change. Cambridge University Press, NY.